Operational Planning of Active Distribution Grids under Uncertainty

Stavros Karagiannopoulos*, Line Roald†, Petros Aristidou‡, Gabriela Hug*
* EEH - Power Systems Laboratory, ETH Zurich, Physikstrasse 3, 8092 Zurich, Switzerland
† Los Alamos National Laboratory, Los Alamos, NM 87545
‡ School of Electronic and Electrical Engineering, University of Leeds, Leeds LS2 9JT, UK
Emails: {karagiannopoulos, hug}@eeh.ee.ethz.ch, roald@lanl.gov, p.aristidou@leeds.ac.uk

***Abstract*—Modern distribution system operators are facing constantly changing operating conditions caused by the increased penetration of intermittent renewable generators and other distributed energy resources. Under these conditions, the distribution system operators are required to operate their networks with increased uncertainty, while ensuring optimal, cost-effective, and secure operation. This paper proposes a centralized scheme for the operational planning of active distribution networks under uncertainty. A multi-period optimal power flow algorithm is used to compute optimal set-points of the controllable distributed energy resources located in the system and ensure its security. Computational tractability of the algorithm and feasibility of the resulting flows are ensured with the use of an iterative power flow method. The system uncertainty, caused by forecasting errors of renewables, is handled through the incorporation of chance constraints, which limit the probability of insecure operation. The resulting operational planning scheme is tested on a low-voltage distribution network model using real forecasting data for the renewable energy sources. We observe that the proposed method prevents insecure operation through efficient use of system controls.**

***Index Terms*—active distribution network, chance constrained multi-period optimal power flow, backward forward sweep power flow, distributed energy resources**

I. Introduction

The increasing penetration of Distributed Energy Resources (DERs) in medium and Low Voltage (LV) distribution networks is posing new challenges to system operation, while at the same time creating exciting new opportunities. On the one hand, large shares of renewables, such as wind and photovoltaic generation (PVs), lead to increased power flow variability due to fluctuations of the injections. This is forcing Distribution Network Operators (DNOs) to operate under increased uncertainty and at higher risks. On the other hand, controllable DERs, such as Battery Energy Storage Systems (BESS), flexible loads, and dispatchable inverter-based Distributed Generators (DGs), provide new sources of flexibility. In active distribution networks, the DERs are requested by the DNO to provide ancillary services, making the distribution network operation more efficient and providing the tools to handle increased uncertainty and increased load.

Ancillary services provided by DERs include among others reactive power control [1], active power curtailment [2], network upgrade deferral by means of BESS [3], and load shifting [4]. To tackle voltage or congestion problems in distribution networks, reactive power control is usually preferred. By adjusting the reactive power injection of DERs, DNOs can perform voltage control or decrease the flow over congested lines. In certain cases, for example when DERs are obliged to operate at unity power factor or the system has a high R/X ratio, reactive power control might be less effective for voltage regulation. In these situations, active power curtailment can be used as an additional means of alleviating the aforementioned problems. However, curtailing active power typically incurs a higher compensation cost to be paid by the DNO. Finally, a combination of reactive and active power control can be used, taking into account both the DER characteristics [3], [5] and the grid rules, to achieve an optimal or near optimal operation of distribution networks.

Based on the communication infrastructure available for controlling the DERs, operation schemes can be generally characterized as centralized or decentralized. In decentralized schemes, e.g. [1], [2], local control strategies are employed to tackle power quality issues, without the use of communication to coordinate the units. Thus, only local information is used to modify the DER behaviour. Centralized distribution grid optimization, used for active distribution grid operation, has lately attracted significant attention thanks to advances in computational power and new theoretical developments in approximations of the nonlinear AC power flow equations. In centralized schemes, e.g. [6], [7], a central entity makes use of communication infrastructure to gather information from local DERs and employ network-level optimization to provide system-wide optimal settings for the controlled DERs. Lately, hybrid schemes have been proposed, e.g. [8], that apply off-line, centralized optimization to derive optimized local control schemes that can be applied when little or no communication infrastructure is available.

In this paper, we investigate a centralized scheme for operating a distribution network with large shares of renewables under uncertainty. The method employs optimization techniques that exploit system-wide information about the network and consider the impact of uncertainty to derive optimal DER setpoints by running a multi-period, chance-constrained Optimal Power Flow (OPF).

II. Related work and Contributions

In this section, we review related work in distribution network optimization. We consider three different aspects: a) the available active measures for distribution network control, b) the choice of power flow representation and c) the methods to account for uncertainty. We then describe the distinguishing contributions of our work.

a) Active Measures Considered: A variety of measures for distribution network control are considered in the literature. Many references use only one active measure, such as active power curtailment [2], reactive power control [9], controllable loads [4], etc., while others use a combination of control measures, e.g. active power curtailment and reactive power control [7], [8], [10], [11], active power curtailment, reactive power control and BESS [12], [13] or active power curtailment, reactive power control, BESS and controllable loads [3]. In this work, we consider a combination of active power curtailment, reactive power control, BESS and controllable loads. In addition, we include controllable On Load Tap Changing (OLTC) transformers that can control the voltage magnitude of the transformer.

b) Power Flow Equations: The DC power flow approximation, which is used widely in transmission grid studies, is not suitable for distribution networks since the line resistances are not negligible and the voltage magnitudes are typically not close to nominal. At the same time, the use of the non-convex non-linear AC power flows in an OPF framework, as in [7], can easily become computationally complex. Convex relaxations, based on e.g. semidefinite relaxations [14], find solutions that are globally optimal for the original problem in many practical cases. However, using a relaxation might lead to an optimization outcome which is not a physically valid solution to the original AC power flow equations. Moreover, the computational complexity of the convex relaxations is still high [10], [11]. By exploiting the radial or weakly meshed distribution network topology, it is possible to solve the power flow problem using the iterative backward and/or forward sweep (BFS) power flow method [15], as shown in [3], [6]. In this paper, we apply a modified version of the BFS-OPF to ensure computational tractability and feasibility of the multi-period OPF problem.

c) Uncertainty modeling: The increasing penetration of renewable, distributed, generation has increased the level of uncertainty in distribution networks. The safe integration of uncertain resources has hence gained a lot of attention, both in the transmission and distribution grids. Recent papers use tools from risk-aware portfolio optimization [11] or rely on single [11], [13], [16]–[19] or joint [20], [21] chance constraints to ensure that the corresponding limits will be enforced with a pre-described probability to limit possible adverse impacts of uncertainty. To reformulate the chance constraints into a tractable representation, some methods assume a certain (Gaussian) distribution of the forecast error and provide an analytical reformulation [11], [13], [16], [18], while others are distribution agnostic [19]–[21]. In this work, we consider single chance constraints, and use an iterative solution scheme [18], [22] to enforce these constraints. The iterative scheme is based on the observation that the chance constrained problem can be interpreted as a deterministic problem with tightened constraints, where the optimal tightening, which strikes the best trade-off between cost and system security, is a function of the optimization variables. The iterative scheme alternates between solving the deterministic problem with a given set of tightenings, and evaluating the optimal constraint tightening based on the solution of the deterministic problem. A feasible solution is found when the tightenings do not change between iterations. The benefit of the iterative approach is that the evaluation of the constraint tightenings is done outside of the optimization problem. This enables the use of accurate, but computationally heavy evaluation methods, such as Monte Carlo simulations [22]. Using a Monte Carlo simulation based on samples of the uncertain variables allows us to obtain accurate values for the tightenings, without making limiting assumptions about the system equations or the distribution of the generation from the DERs.

This paper proposes a multi-period OPF formulation for the operational planning of active distribution grids under uncertainty. The contributions of this paper are twofold:

1) We extend previous modelling of active distribution network operations:
   - We include a wider range of measures for active control, considering not only active power curtailment, reactive power control, BESS and controllable loads, but also OLTC transformers.
   - We apply the BFS power flow algorithm to ensure tractability, but make some modifications to previous schemes to improve feasibility.
   - We mitigate adverse impacts of forecast error uncertainty by formulating a chance constrained problem, which is reformulated based on a Monte Carlo approach and solved using an iterative solution scheme.
2) We investigate the added benefit of the control through a case study. We compare the behavior of different sets of available active measures and we investigate the impact of considering uncertainties on constraint violations and on costs.

The remainder of the paper is organized as follows: Section III presents the general mathematical formulation of the deterministic multi-period AC-OPF considering the modeling of active measures. Section IV describes the principles of the iterative BFS power flow method and the incorporation of BFS within the multi-period OPF, while Section V explains the modeling of PV uncertainty, as well as the formulation using chance constraints. Section VI summarizes the overall solution algorithm, while Section VII introduces the considered case study and the simulation results. Finally, conclusions are drawn in Section VIII.

III. Operational Planning of Distribution Grids

In this section, we detail the modeling of the deterministic multi-period OPF problem formulation including the full, non-

linear AC power flow equations. We describe the objective, as well as the constraints on power balance, on power quality and on active measures.

A. Formulation of the Deterministic Multi-period Optimal Power Flow

We consider a distribution network with a set of nodes $\mathcal{J} := 1, 2, ..., N_b$ (denoted by index j) and a set of lines $\mathcal{I} := 1, 2, ..., N_{br}$ (denoted by index i). In order to account for the inter-temporal constraints of DERs and the OLTC transformer, we need to solve the following multi-period AC OPF over the time horizon $\mathcal{T} := 1, ..., N_{hor}$ (with each timestep denoted by index t):

$$\min_{\mathbf{u}} \; c(\mathbf{x}, \mathbf{u}) \tag{1a}$$

$$\text{s.t.} \quad f(\mathbf{x}, \mathbf{u}, \mathbf{y}) = 0 \qquad \forall j, t \in \mathcal{J}, \mathcal{T}, \tag{1b}$$

$$h_V(\mathbf{x}, \mathbf{u}, \mathbf{y}) \leq 0 \qquad \forall j, t \in \mathcal{J}, \mathcal{T}, \tag{1c}$$

$$h_I(\mathbf{x}, \mathbf{u}, \mathbf{y}) \leq 0 \qquad \forall i, t \in \mathcal{I}, \mathcal{T}, \tag{1d}$$

$$h_{\text{DER}}(\mathbf{x}, \mathbf{u}, \mathbf{y}) \leq 0 \qquad \forall j, t \in \mathcal{J}, \mathcal{T}, \tag{1e}$$

$$g_{\text{DER}}(\mathbf{x}, \mathbf{u}, \mathbf{y}) = 0 \qquad \forall j, t \in \mathcal{J}, \mathcal{T}. \tag{1f}$$

Here, $\mathbf{u}$ represents the control vector, e.g. the DER active and reactive power setpoints, the position of the transformer taps, etc.; $\mathbf{x}$ corresponds to the state vector, i.e. the bus voltage magnitudes and angles (except for the slack bus, where the angle is set to 0 degrees and the magnitude is fixed); and $\mathbf{y}$ defines the constant parameters vector, comprising of the network topology, physical characteristics of the grid, and the thermal and voltage constraint limits.

The DNO optimizes the control vector $\mathbf{u}$ over the objective function (1a), where the function $c(\mathbf{x}, \mathbf{u})$ represents the combined cost of the required control measures and the cost of covering the losses.

Equation (1b) corresponds to the standard AC power flow equations enforcing active and reactive power balances at each node. It is a function of the states $|V|$, Θ, denoting the voltage magnitudes and angles, and P_{inj}, Q_{inj} denoting the nodal injections of active and reactive power. Equations (1c)-(1d) ensure that the voltage and current magnitudes remain within acceptable limits, and (1e)-(1f) refer to DER models and constraints.

In the following sections, we will elaborate on the objective function and the modeling of all available active measures used in this work, i.e. the DERs and OLTC transformer.

1) Objective function-(1a): The objective of the DNO is to minimize its operating costs, associated with the cost of DER control to guarantee a safe grid operation, and network losses. In this work, the cost of DER control is determined based on the curtailment of active energy and provision of reactive power support by DGs. We assume that the other active measures (such as BESS, OLTC transformer and load control) do not incur operational cost to the DNO. In the general case, their cost can be easily included in the objective function. The objective function is evaluated by summing the cost of DER control over all network nodes N_b, branches N_{br} and the entire time horizon N_{hor},

$$\min_{\mathbf{u}} \sum_{t=1}^{N_{\text{hor}}} \left(\sum_{j=1}^{N_{\text{b}}} (c_{\text{P}}^T \cdot P_{\text{curt,j,t}} + c_{\text{Q}}^T \cdot Q_{\text{ctrl,j,t}}) + \underbrace{\sum_{i=1}^{N_{\text{br}}} c_{\text{P}}^T \cdot P_{\text{loss,i,t}}}_{\text{losses}} \right) \Delta t, \tag{2}$$

where Δt is the length of each time period. The curtailed power of the DG at node j and time t is given by $P_{\text{curt,j,t}} = P_{\text{g,j,t}}^{\text{max}} - P_{\text{g,j,t}}^{\text{f}}$, where $P_{\text{g,j,t}}^{\text{max}}$ is the maximum available active power and $P_{\text{g,j,t}}^{\text{f}}$ is the actual infeed. The use of the reactive power support $Q_{\text{g,j,t}}^{\text{f}}$ for each DG at node j and time t is minimized by including the term $Q_{\text{ctrl,j,t}} = |Q_{\text{g,j,t}}^{\text{f}}|$ in the objective function. The losses in each branch i at time t are calculated by $P_{\text{loss,i,t}} = |I_{\text{br,i,t}}|^2 \cdot R_{\text{br,i}}$, where $|I_{\text{br,i,t}}|$ is the magnitude of the current flow and $R_{\text{br,i}}$ its resistance. Finally, the coefficients c_{P}^T and c_{Q}^T represent, respectively, the DG cost of curtailing active power and providing reactive power support. Selecting $c_{\text{Q}}^T \ll c_{\text{P}}^T$ prioritizes the use of reactive power control over active power curtailment.

2) Power balance constraints-(1b): The power injection equations at every node j and time step t are given by

$$P_{\text{inj,j,t}}^{\text{f}} = P_{\text{g,j,t}}^{\text{f}} - P_{\text{lflex,j,t}}^{\text{f}} - (P_{\text{B,j,t}}^{\text{ch}} - P_{\text{B,j,t}}^{\text{dis}}), \tag{3a}$$

$$Q_{\text{inj,j,t}}^{\text{f}} = Q_{\text{g,j,t}}^{\text{f}} - P_{\text{lflex,j,t}}^{\text{f}} \cdot tan(\phi_{\text{load}}). \tag{3b}$$

For each node j and time step t, $P_{\text{inj,j,t}}^{\text{f}}$ and $Q_{\text{inj,j,t}}^{\text{f}}$ are the net active and reactive power injections of the nodes. $P_{\text{g,j,t}}^{\text{f}}$ and $Q_{\text{g,j,t}}^{\text{f}}$ are the active and reactive power infeeds of the DGs; $P_{\text{lflex,j,t}}^{\text{f}}$ and $P_{\text{lflex,j,t}}^{\text{f}} \cdot tan(\phi_{\text{load}})$ are the active and reactive node demands (after control), with $cos(\phi_{\text{load}})$ being the power factor of the load; $P_{\text{B,j,t}}^{\text{ch}}$ and $P_{\text{B,j,t}}^{\text{dis}}$ are respectively the charging and discharging power of the BESS. The nodal power balance equations using the full, non-linear AC power flow are given by

$$P_{\text{inj,j,t}}^{\text{f}} = |V_{\text{bus,k,t}}| \sum_{m=1}^{N_b} |V_{\text{bus,m,t}}| (G_{\text{km}} cos\theta_{\text{km,t}} + B_{\text{km}} sin\theta_{\text{km,t}}), \tag{4a}$$

$$Q_{\text{inj,j,t}}^{\text{f}} = |V_{\text{bus,k,t}}| \sum_{m=1}^{N_b} |V_{\text{bus,m,t}}| (G_{\text{km}} sin\theta_{\text{km,t}} - B_{\text{km}} cos\theta_{\text{km,t}}). \tag{4b}$$

Here, $G_{\text{km}} + jB_{\text{km}} = Y_{\text{km}}$ form the nodal admittance matrix, $|V_{\text{bus,k,t}}|, |V_{\text{bus,m,t}}|$ are the voltage magnitudes at buses k and m respectively, and $\theta_{\text{km,t}} = \theta_{\text{k,t}} - \theta_{\text{m,t}}$ is the voltage angle difference between these buses, both at time t.

3) Power quality constraints-(1c,1d): The voltage constraints for each bus j and the current constraints for each line i, for each time step t, are given by

$$V_{\text{min}} \leq |V_{\text{bus,j,t}}| \leq V_{\text{max}}, \tag{5a}$$

$$|V_{\text{slack}}| = 1, \quad \theta_1 = 0, \tag{5b}$$

$$|I_{\text{br,i,t}}| \leq I_{\text{i,max}}, \tag{6}$$

where $|V_{\text{slack}}|$ and $|V_{\text{bus,j,t}}|$ are the voltage magnitudes at the slack and all other buses respectively, and V_{max}, V_{min} the upper and lower acceptable voltage limits; the slack bus voltage angle, i.e. θ_1 is set to zero degrees; and $I_{\text{i,max}}$ is its maximum thermal limit.

Since this work focuses on distribution networks, the slack bus is the bus on the high voltage side of the distribution transformer, which can be equipped with OLTC capabilities. The operation and constraints of the OLTC transformer are modelled as

$$|V_{\text{LV-trfo}}| = |V_{\text{slack}} - \Delta V_{\text{tap}} \cdot \rho_{\text{t}}|, \tag{7a}$$

$$\sum_{t=2}^{24}(|\rho_{\text{t}} - \rho_{\text{t-1}}|) \leq 2, \tag{7b}$$

$$\rho_{min} \leq \rho_{\text{t}} \leq \rho_{max}, \tag{7c}$$

where $|\Delta V_{tap}|$ is the voltage magnitude change caused by one tap switching action of the OLTC transformer (assumed constant for simplicity), ρ_{t} is an integer value defining the position of the tap, and $V_{\text{LV-trfo}}$ is the voltage on the low-voltage side of the transformer. Constraint (7b) assures that there is a maximum of two tap switching actions within a day to avoid wear and tear on the transformer, and the parameters $(\rho_{\text{min}}, \rho_{\text{max}})$ in (7c) define the minimum and maximum tap positions of the OLTC transformer.

4) Active measures constraints-(1e,1f):

a) DG limits: In this work, we consider inverter-based DGs such as PVs. The limits are given by

$$P^{\text{min}}_{\text{g,j,t}} \leq P^{\text{f}}_{\text{g,j,t}} \leq P^{\text{max}}_{\text{g,j,t}}, \tag{8a}$$

$$-\tan(\phi_{\text{max}}) \cdot P^{\text{f}}_{\text{g,j,t}} \leq Q^{\text{f}}_{\text{g,j,t}} \leq \tan(\phi_{\text{max}}) \cdot P^{\text{f}}_{\text{g,j,t}}, \tag{8b}$$

where $P^{\text{min}}_{\text{g,j,t}}$ and $P^{\text{max}}_{\text{g,j,t}}$ are the upper and lower limits for active DG power at each node j and time t. These limits vary depending on the type of the DG and the control schemes implemented. Usually, small DGs have technical or regulatory [23] limitations on the power factor they can operate at. Here, we use the reactive power limit given in (8b), which limits the reactive power output as a function of the maximum power factor $cos(\phi_{\text{max}})$.

b) Controllable loads: We consider flexible loads with an on/off controllable nature, i.e loads which can shift a fixed amount of power over some time. The behavior of such loads at each controllable node j is given by

$$P_{\text{lflex,j,t}} = P_{\text{l,j,t}} + z_{\text{j,t}} \cdot P_{\text{shift,j}}, \quad -1 \leq z_{\text{j,t}} \leq 1, \tag{9a}$$

$$\sum_{t=1}^{24} z_{\text{j,t}} = 0, \tag{9b}$$

where $P_{\text{lflex,j,t}}$ is the final controlled active demand at node j and time t, $P_{\text{shift,j}}$ is the constant shiftable load at node j and $z_{\text{j,t}} \in \{-1, 0, 1\}$ is an integer variable indicating an increase or a decrease of the load when shifted from the known initial demand $P_{\text{l,j,t}}$. Constraint (9b) assures that the final total daily energy demand is maintained.

c) Battery Energy Storage Systems: Finally, the constraints related to the BESS are given as

$$SoC^{\text{bat}}_{\text{min}} \cdot E^{\text{bat}}_{\text{inv,j}} \leq E^{\text{bat}}_{\text{j,t}} \leq SoC^{\text{bat}}_{\text{max}} \cdot E^{\text{bat}}_{\text{inv,j}}, \tag{10a}$$

$$E^{\text{bat}}_{\text{j,1}} = E_{\text{start}}, \tag{10b}$$

$$E^{\text{bat}}_{\text{j,t}} = E^{\text{bat}}_{\text{j,t-1}} + (\eta_{\text{bat}} \cdot P^{\text{ch}}_{\text{B,j,t}} - \frac{P^{\text{dis}}_{\text{B,j,t}}}{\eta_{\text{bat}}}) \cdot \Delta t, \tag{10c}$$

$$P^{\text{ch}}_{\text{B,j,t}} \geq 0, \quad P^{\text{dis}}_{\text{B,j,t}} \geq 0, \tag{10d}$$

$$P^{\text{ch}}_{\text{B,j,t}} \cdot P^{\text{dis}}_{\text{B,j,t}} \leq \hat{\eta}. \tag{10e}$$

Here, $E^{\text{bat}}_{\text{inv,j}}$ is the installed BESS capacity at node j, $SoC^{\text{bat}}_{\text{min}}$, $SoC^{\text{bat}}_{\text{max}}$ are the fixed minimum and maximum per unit limits for the battery state of charge, and $E^{\text{bat}}_{\text{j,t}}$ is the available energy capacity at node j and time t. The initial energy content of the BESS in time period 1 is given by E_{start}, and (10c) updates the energy capacity at each time step t based on the BESS efficiency η_{bat}, time interval Δt and the charging and discharging power of the BESS $P^{\text{ch}}_{\text{B,j,t}}$ and $P^{\text{dis}}_{\text{B,j,t}}$. The charging and discharging power are defined as positive according to (10d). Equation (10e) ensures that the BESS is not charging and discharging at the same time, by using an arbitrarily small value $\hat{\eta} = 10^{-5}$.

In order to avoid the bi-linearity of (10e), we replace the constraint with

$$P^{\text{ch}}_{\text{B,j,t}} \cdot (P_{\text{l,j,t}} - P^{\text{max}}_{\text{g,j,t}}) \leq \hat{\eta}, \tag{10f}$$

$$P^{\text{dis}}_{\text{B,j,t}} \cdot (P_{\text{l,j,t}} - P^{\text{max}}_{\text{g,j,t}}) \geq \hat{\eta}. \tag{10g}$$

Here, we make the assumption that when excess (deficit) of generation is expected locally, the BESS at that node is not allowed to discharge (charge) [24].

IV. Backward/Forward Sweep Power Flow Method

Distribution networks differ from transmission grids in that they are typically radially operated and have high R/X ratio. Furthermore, the loading at the three phases is unbalanced and the lines/cables are not transposed. Due to these differences, some conventional power flow methods may be inefficient for the distribution networks. However, other solution methods, such as the BFS power flow method considered in this work, exploit the radial or weakly meshed distribution grid topology to increase efficiency.

By considering the full AC power balance equations in the OPF problem, the inter-temporal constraints of many active measures (OLTC transformer, BESS, controllable loads, etc.), and the integer variables of the controllable loads and the tap position, the problem can easily solve slowly or become computationally complex. To tackle this problem, we replace the full power flow equations in the OPF formulation with a single iteration of the BFS method. After the OPF solution, we perform an exact BFS power flow computation. In this way, we obtain a solution to the full, non-linear set of AC power flow equations for the chosen set of controls. In the next iteration, we again solve the OPF problem, starting from the AC feasible solution for the previous set of controls. In this section, we present the BFS power flow technique and its incorporation into the OPF framework.

A. BFS power flow solution

The basic formulation of the BFS used in this work is taken from [15] and is shown in Algorithm 1. The solution of the power flow problem is achieved by iteratively "sweeping" the distribution network and updating the network variables at each iteration. The structure of the grid is captured by two matrices: the Bus Injection to Branch Current (BIBC), and the Branch Current to Bus Voltage (BCBV) matrices. BIBC is a matrix with real elements composed of ones and zeros, capturing the topology of a given network, whereas BCBV is a matrix with the complex impedance of the lines as elements. One iteration of the algorithm consists of two sweeps. First, in the backward sweep step of the k^{th} BFS iteration, the current injections at all buses are calculated (11a) and the corresponding branch currents are computed using the BIBC matrix (11b), i.e.

$$I_{\text{inj}}^{k} = \left(\frac{(P_{\text{inj}} + jQ_{\text{inj}})^{*}}{V_{\text{bus}}^{k*}} \right), \tag{11a}$$

$$I_{\text{br}}^{k} = BIBC \cdot I_{\text{inj}}^{k}. \tag{11b}$$

where I_{inj}^{k} and I_{br}^{k} are the complex current injections at all buses and flows at all branches respectively. Then, in the forward sweep step, the currents are used to calculate the voltage drop over all branches using BCBV (12a), and the bus voltages are updated for the next iteration (12b) as follows

$$\Delta V^{k+1} = BCBV \cdot I_{\text{br}}^{k}, \tag{12a}$$

$$V_{\text{bus}}^{k+1} = V_{\text{slack}} - \Delta V_{\text{tap}} \cdot \rho_{\text{t}} + \Delta V^{k+1}. \tag{12b}$$

In LV grids, it is the voltage magnitude differences that dictate the flows in the lines/cables and the voltage angles are typically small, due to the high R/X ratio. Thus, a reasonable approximation for LV grids would be to consider only the real part of the voltage drop. In this case, (12a) can be substituted by

$$\Delta V^{k+1} \approx Re\left\{ BCBV \cdot I_{\text{br}}^{k} \right\}. \tag{13}$$

This assumption, i.e. assuming zero voltage angles and thus considering only the real voltage drop, is reasonable for LV networks [6], where the angles are typically below 10°. The algorithm converges when the maximum voltage magnitude difference between two subsequent iterations is smaller than a predetermined threshold $\bar{\eta}$.

Algorithm 1 Main steps of BFS power flow based on [15]

Input: BIBC, BCBV, $P_{\text{inj}}, Q_{\text{inj}}$, V_{slack}
Output: I_{br}^{k}, V_{bus}^{k+1}
initialize: $k = 1$, $V_{\text{bus}}^{k} = 1\angle 0°$
do
  Backward sweep: $I_{\text{inj}}^{k} = \left(\frac{(P_{\text{inj}} + jQ_{\text{inj}})^{*}}{V_{\text{bus}}^{k*}} \right)$
  $I_{\text{br}}^{k} = BIBC \cdot I_{\text{inj}}^{k}$
  Forward sweep: $\Delta V^{k+1} = BCBV \cdot I_{\text{br}}^{k}$
  $V_{\text{bus}}^{k+1} = V_{\text{slack}} - \Delta V_{\text{tap}} \cdot \rho_{\text{t}} + \Delta V^{k+1}$
  Update iteration: $k+ = 1$
while $max|(|V_{\text{bus}}^{k}| - |V_{\text{bus}}^{k-1}|)| \geq \bar{\eta}$
return I_{br}^{k}, V_{bus}^{k}

B. BFS-OPF implementation

To incorporate the BFS-based power balance equations into our OPF framework, (4a)-(4b) are replaced by a single sweeping iteration of the BFS method. Thus, using (11), the constraint for the current magnitude for all branches i, at each iteration k and time step t, is given by

$$|I_{\text{br,i,t}}^{\text{k}}| \leq I_{\text{i,max}}. \tag{14a}$$

Furthermore, considering also the OLTC capabilities (7a), the equations for the voltage magnitudes at all nodes are now given by (12b). According to (13), we can consider only the real part of the voltage drop, approximating the voltages with $V_{\text{bus,j,t}}^{\text{k}} \approx V_{\text{slack}} - \Delta V_{\text{tap}} \cdot \rho_{\text{t}} + Re\left\{\Delta V^{k+1}\right\}$, where all elements have zero imaginary part. Therefore, considering the magnitude $|V_{\text{bus,j,t}}^{\text{k}}| \approx V_{\text{slack}} - \Delta V_{\text{tap}} \cdot \rho_{\text{t}} + Re\left\{\Delta V^{k+1}\right\}$, we end up with a linear voltage constraint inside the OPF formulation, given by

$$V_{\text{min}} \leq V_{\text{slack}} - \Delta V_{\text{tap}} \cdot \rho_{\text{t}} + Re\left\{\Delta V^{k+1}\right\} \leq V_{\text{max}}. \tag{15}$$

By considering this approximation, we avoid the use of the non-convex exact AC power flow, and we solve the OPF with one BFS iteration. After the optimal setpoints of the OPF problem are obtained, the exact BFS power flow is performed to update the operating point and project it into the feasible domain of the exact power flow equations. This new operating point will be used as input to the subsequent iteration of the BFS-OPF problem, and this loop will be repeated until convergence in terms of voltage magnitude mismatch. This procedure is sketched in Fig. 5, labeled as *multi-period BFS-OPF*.

This approach is in contrast to [6] where only one BFS iteration is performed after the OPF solution. The formulation used in this work fully computes the voltages and currents after each OPF solution and can improve (or facilitate) the convergence of the BFS-OPF, especially when the current operating point is far from the optimum or close to the stability limits and a single BFS iteration would not give a good approximate of the values.

V. Accounting for Uncertainty through Chance Constraints

With the above formulation, we have a tractable optimization problem for the multi-period OPF. What remains is to account for the effect of uncertainty, and formulate a problem that limits possible adverse effects.

Uncertainty is becoming an important issue for distribution grids due to increasing installations with variable output, e.g. wind farms in medium voltage and PV panels in LV grids, respectively. This work focuses on LV networks and thus, assumes that the power injection from the PV units is the only uncertainty source. However, load uncertainty could be modelled and included in the optimization problem in a similar way, without requiring any extensions to the method.

A. Formulation of the Chance Constraints

In order to mitigate the effect of uncertainty on system operation, is is necessary to account for uncertainty within the optimization framework. In our model, the branch current flows and the voltage magnitudes are functions of the power injections and are hence influenced by PV power uncertainty. To limit the risk of constraint violations, we model the corresponding voltage and current constraints as chance constraints. Chance constraints are probabilistic constraints which ensure that the limits will hold with a pre-described probability 1 - ε, where ε is the acceptable violation probability. With this definition, the voltage constraints (5a) and current constraints (6) become

$$\mathbb{P}\left\{|V_{\text{bus,j,t}}| \leq V_{\text{max}}\right\} \geq 1-\varepsilon, \tag{16}$$
$$\mathbb{P}\left\{|V_{\text{bus,j,t}}| \geq V_{\text{min}}\right\} \geq 1-\varepsilon, \tag{17}$$
$$\mathbb{P}\left\{|I_{\text{br,i,t}}| \leq I_{\text{i,max}}\right\} \geq 1-\varepsilon. \tag{18}$$

The probabilistic constraints (16) - (18) are not tractable in their current form, and require reformulation into deterministic constraints. This can be done by interpreting them as tightened versions of the original constraints [16], [22], where the tightening represents a security margin against uncertainty, i.e., an *uncertainty margin*. Using this observation, it is possible to express (16), (18) as

$$V_{\text{min}} + \Omega^{\text{lower}}_{\text{V j,t}} \leq |V^{\text{k}}_{\text{bus,j,t}}| \leq V_{\text{max}} - \Omega^{\text{upper}}_{\text{V j,t}}, \tag{19}$$
$$|I^{\text{k}}_{\text{br,i,t}}| \leq I_{\text{i,max}} - \Omega_{I_{\text{br,i}}}, \tag{20}$$

where $\Omega^{\text{lower}}_{\text{V}}$, $\Omega^{\text{upper}}_{\text{V}}$ are the tightenings for the lower and upper voltage magnitude constraints and $\Omega_{I_{\text{br}}}$ are the tightenings of the current magnitude constraints. Figures 1 and 2 schematically show the uncertainty margins on the voltage and current flow constraints due to the introduction of the uncertainty sets.

B. Iterative Solution Algorithm

Since the effect of the uncertainty is captured in the uncertainty margins and does not occur elsewhere in the problem, it is possible to solve the problem using an iterative algorithm [18], [22]. The iterative algorithm for AC chance-constrained OPF alternates between solving a deterministic OPF with tightened constraints, and calculating the uncertainty margins $\Omega^{\text{lower}}_{\text{V}}$, $\Omega^{\text{upper}}_{\text{V}}$, $\Omega_{I_{\text{br}}}$ based on the obtained solution. If the maximum changes in the tightenings between two subsequent iterations are below certain thresholds η^{Ω}_{V}, η^{Ω}_{I}, the algorithm has converged and a feasible solution has been found. This procedure is sketched in Fig. 5 in the green box labeled *Uncertainty tightenings*.

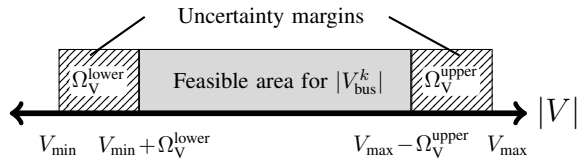

Fig. 1. Voltage constraint tightening due to the uncertainty margins.

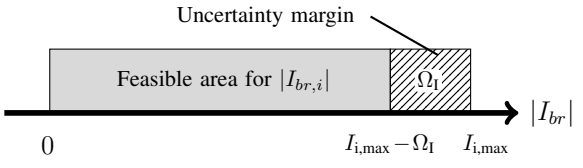

Fig. 2. Maximum current tightening due to the uncertainty margin.

C. Evaluation based on Monte Carlo Simulations

The iterative algorithm, which evaluates the uncertainty margins in an outer iteration and not within the OPF problem itself, enables several ways of obtaining the uncertainty margins $\Omega^{\text{lower}}_{\text{V}}$, $\Omega^{\text{upper}}_{\text{V}}$, $\Omega_{I_{\text{br}}}$. One approach is to use the analytical reformulation approach based on linear sensitivity factors and the assumption of a Gaussian distribution [17], or related analytical methods that are distribution agnostic [19], [25]. Another approach, which is possible due to the iterative nature of the solution, is to use a Monte Carlo simulation [22]. This method has the benefit that it accounts for the full non-linearity of the AC power flow equations and requires no restrictive (or conservative) assumptions about the uncertainty distribution. If a sufficient number of representative samples is available, we are able to get a very accurate estimate of the necessary uncertainty margins.

The calculation procedure for the Monte Carlo based tightenings is summarized in Fig. 3 and Fig. 4. Given the optimal set-points from the BFS-OPF, the Monte Carlo simulations are used to calculate an empirical distribution function for the voltages and currents at each time step. Since we consider separate chance constraints, each constraint has its own empirical distribution as depicted schematically for a voltage constraint in Fig. 4. Enforcing a chance constraint with $1-\epsilon$ probability is equivalent to ensuring that the $1-\epsilon$ quantile of the distribution remains within bounds. Hence, the tightening corresponds to the difference between the forecasted voltage magnitude at zero forecast error $|V^{\text{k,0}}_{\text{bus,j,t}}|$ and the $1-\epsilon$ quantile $V^{\text{k,1-}\epsilon\%}_{\text{bus,j,t}}$.

The upper $1-\epsilon$ quantile $V^{\text{k,1-}\epsilon\%}_{\text{bus,j,t}}$ and the lower ϵ quantile $V^{\text{k,}\epsilon\%}_{\text{bus,j,t}}$ of the voltage magnitudes, as well as the $1-\epsilon$ quantile of the current magnitudes are evaluated based on the empirical distribution. The empirical uncertainty margins are then given by

$$\Omega^{\text{upper}}_{\text{V j,t}} = |V^{\text{k,1-}\epsilon}_{\text{bus,j,t}}| - |V^{\text{k,0}}_{\text{bus,j,t}}|, \tag{21a}$$
$$\Omega^{\text{lower}}_{\text{V j,t}} = |V^{\text{k,0}}_{\text{bus,j,t}}| - |V^{\text{k,}\epsilon}_{\text{bus,j,t}}|, \tag{21b}$$
$$\Omega^{\text{upper}}_{I_{\text{br,i}}} = |I^{\text{k,1-}\epsilon}_{\text{br,i,t}}| - |I^{\text{k,0}}_{\text{br,i,t}}|, \tag{21c}$$

where superscript ^{0} indicates the current or voltage magnitude at the operating point with zero forecast error.

VI. Solution Algorithm

In this section, we summarize the proposed method for optimal operational planning of active distribution networks, sketched in Fig. 5.

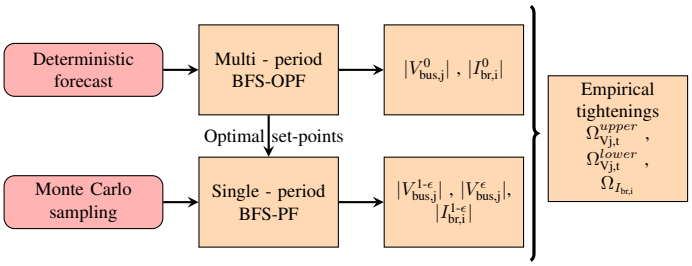

Fig. 3. Procedure to derive the empirical uncertainties sets.

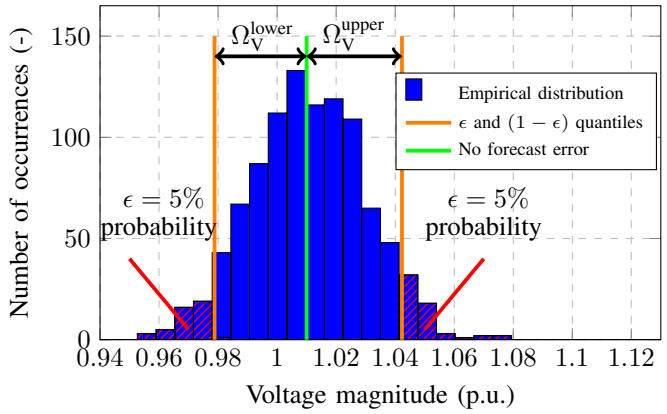

Fig. 4. Example of an empirical distribution for a voltage constraint, with upper and lower tightenings.

At the core of the proposed methodology lies the formulation of the multi-period centralized OPF for active distribution networks described in Section IV. The uncertainty is treated in the outer loop as described in Section V. The initialization stage sets the uncertainty margins to zero and initializes the voltage levels for the multi-period OPF to a flat voltage profile. Then, the BFS-OPF calculates the optimal setpoints of the available active measures based on the first step of the BFS algorithm. The BFS power flow algorithm then runs until convergence for the solution point, and we check whether the converged point is similar to the voltage profile assumed by the OPF. After the multi-period BFS-OPF has converged, the uncertainty margins are evaluated based on the MC approach. The iteration index of the BFS-OPF loop is denoted by k and the iteration of the uncertainty loop by m. The iterative procedure continues until all parts of the algorithm have reached convergence.

VII. Case Study - Results

A. Network description - Case study setup

In order to demonstrate the proposed method, we use the data from the benchmark radial LV grid presented in [26] and shown in Fig. 6. The installed PV capacity is expressed as a percentage of the total maximum load as follows: PV nodes $= [12, 16, 18, 19]$, PV share $(\%) = [45, 40, 30, 45]$. The dimensions of the remaining units used were selected following the planning approach of [3]. More specifically, we consider at node 16 a BESS of 26 kWh, and a flexible load of 5 kW, whose total daily energy consumption needs to be maintained constant. In this work, we only consider balanced, single-phase system operation, but the framework can be extended to three-phase unbalanced networks.

The operational costs are assumed to be $c_{\text{P}} = 0.3\frac{\text{CHF}}{\text{kWh}}$ and $c_{\text{Q}} = 0.01 \cdot c_{\text{P}}$. The BESS cost is considered in the planning stage [3] and thus, the use of the BESS does not incur any operational cost to the DNO.

Regarding the uncertainty modeling, we use historical forecast error distributions and we enforce the chance constraints with an $\varepsilon = 5\%$ violation probability. We assume a maximum acceptable voltage of 1.04 p.u and cable current magnitude of 1 p.u. (on the cable base). The minimum acceptable voltage is set to 0.92 p.u..

Using this system, we investigate the effectiveness of different active control measures and the impact of uncertainty on the network constraint violations and computational burden. To achieve this, we consider different scenarios with incrementally more active control measures provided to the DNO. That is, the first scenario includes only active power curtailment, and the last, all of the control measures described

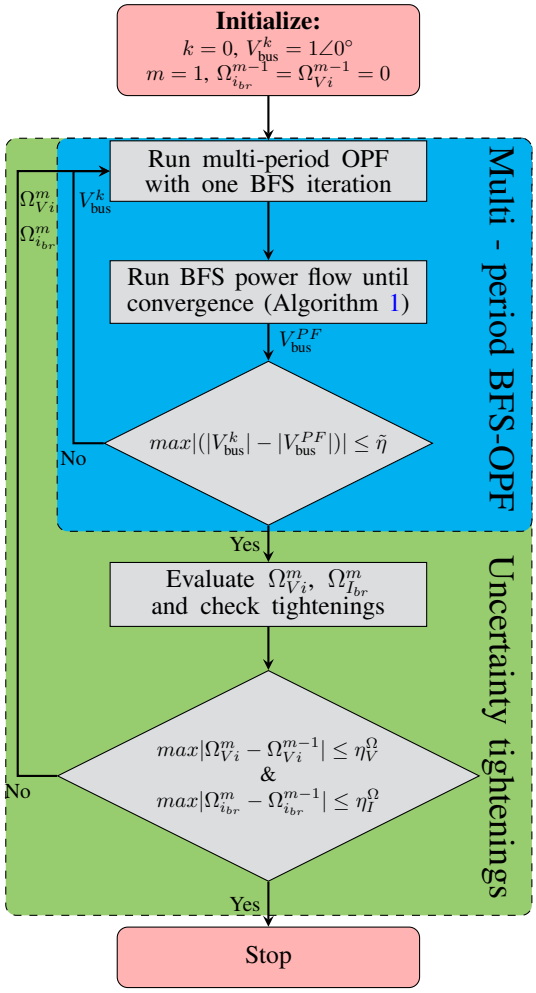

Fig. 5. Proposed solution algorithm.

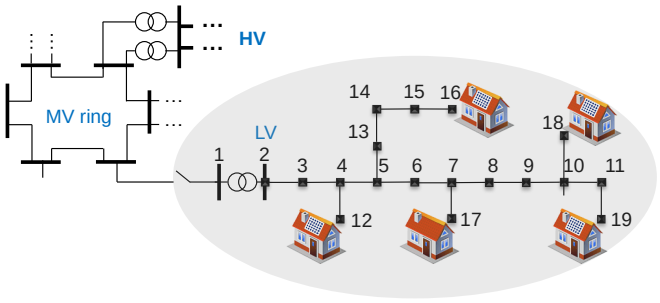

Fig. 6. Cigre LV grid.

in Section III, i.e. active power curtailment, reactive power control, control of BESS, OLTC transformer, and flexible loads. Finally, for each of the above scenarios, we consider a deterministic operational planning approach, the impact of forecasting error, and the benefit of explicitly treating uncertainty through the chance constraints.

B. Forecast error distributions

Reference [27] provides forecasts every 3 hours for 10 PV stations in Switzerland. The goal of this section is to capture forecast error distributions which will serve as inputs to our approach.

Figure 7 shows the histograms of the forecast error distributions of the daily production hours 06:00-20:00 for 9, 6 and 3-hour ahead forecasts for different seasons of the year 2013. As expected, the 3-hour ahead forecasts are more accurate in all cases due to the shorter lead time. These distributions will be used in combination with a new PV injection forecast, to account for uncertainty. The evaluation of the uncertainty margins is carried out based on these samples.

For our case study, we use 1000 samples from the 9-hour ahead forecast error distribution of the summer power profiles as seen in Fig. 7c. We assume a perfect spatial correlation, implying that all PVs follow the same distribution.

C. Optimization results

In this part, we present the results for the operational planning optimization of active distribution networks, for a summer day with high PV infeed. Initially, we show the results without any measures, by running power flow calculations with the forecasted PV injections. Then, we apply the proposed methodology, and we investigate:

- the operational cost and total active power curtailment for different sets of active measures
- the impact of considering uncertainty in the operational cost and violation probabilities
- the computational time and convergence characteristics of the proposed method

1) Base Case - No control measures: In absence of any control action and assuming perfect forecasts, the grid will experience overvoltage and thermal congestion issues, as can be observed by the power flow calculations. Figure 8 shows the

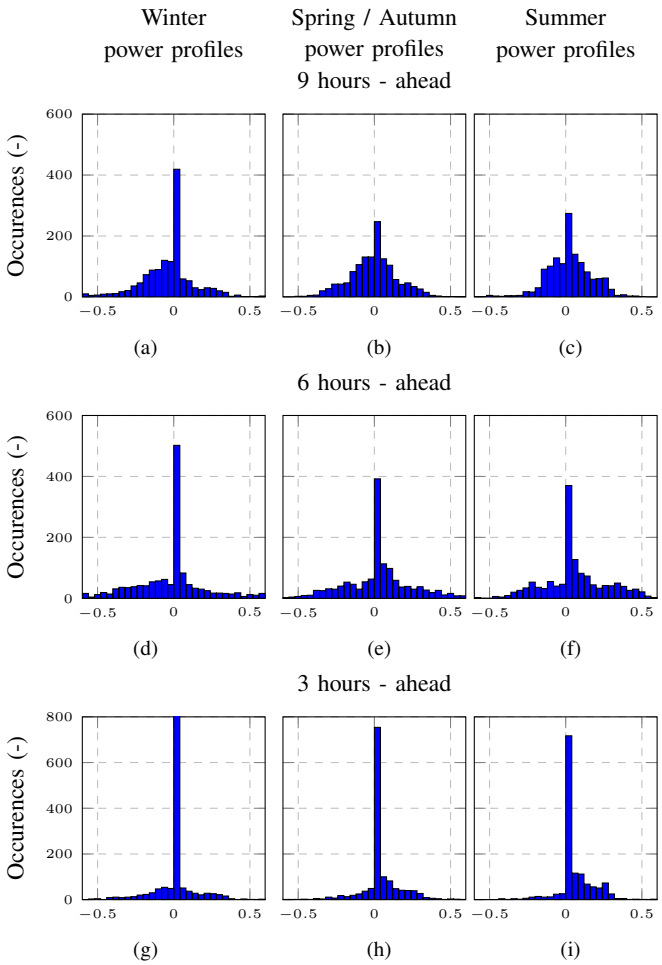

Fig. 7. Histograms of PV forecast errors in p.u. of the installed capacity.

daily voltage magnitude distribution at all nodes. Considering a maximum acceptable voltage magnitude of 1.04 p.u., several nodes face overvoltage issues at noon hours with high solar radiation. Similarly, the boxplots of the thermal loading for all cables shown in Fig. 9, indicate that the cables $2-3$ and $3-4$ will be overloaded. Thus, active control measures are needed to bring the voltages and the currents under acceptable thresholds, leading to a safe grid operation.

2) Optimal scheduling of active distribution grids with different available active measures: The operational flexibility of active measures is used in order to relieve the grid from the aforementioned violations. This section aims at investigating the use of different sets of active measures. More specifically, we quantify the needed control activation and the change of the operational cost as more active measures become available to the DNO.

Figure 10 summarizes the objective function value with and without the consideration of uncertainty. As can be observed, in both cases, the expected cost decreases with more available measures. This occurs due to the decrease of total active power curtailment when other control measures with less operational costs are used, as shown in Table I. At the same time, it can

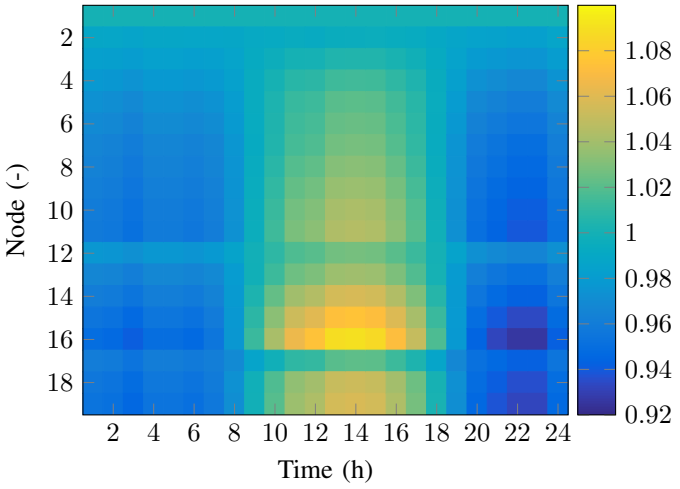

Fig. 8. Daily voltage magnitude distribution at all nodes without any control.

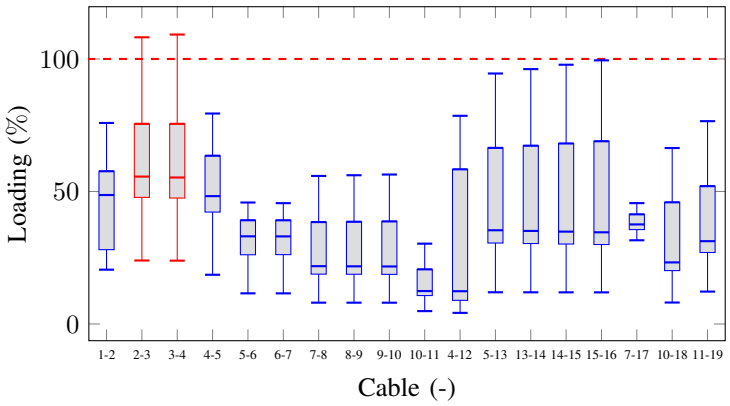

Fig. 9. Boxplots for the daily thermal loading of the cables. Each boxplot shows the minimum, the first quartile, the median, the third quartile, and the maximum value over the time considered.

be seen that the introduction of uncertainty leads to higher curtailment necessary to satisfy the network constraints. In the deterministic case, the total curtailment using only active power curtailment is more than 8 times higher compared to the case with all measures available. A similar pattern is observed in the chance-constrained case, with the use of reactive power control appearing to be the most efficient measure.

3) Impact of considering uncertainty: To highlight the importance of considering the PV injection uncertainty, we provide insights into the distribution of voltage and current magnitudes at specific nodes and cables. We consider the

TABLE I
TOTAL CURTAILMENT NEEDED FOR DIFFERENT SETS OF AVAILABLE ACTIVE MEASURES

Available Measures	Total Active Power Curtailment (% p.u.) Uncertainty	
	Without	With
Active Power Curtailment	10.18	24.83
+ Reactive Power Control	5.28	17.90
+ BESS	4.68	17.27
+ OLTC transformer	2.17	16.48
+ Controllable Load	1.22	15.14

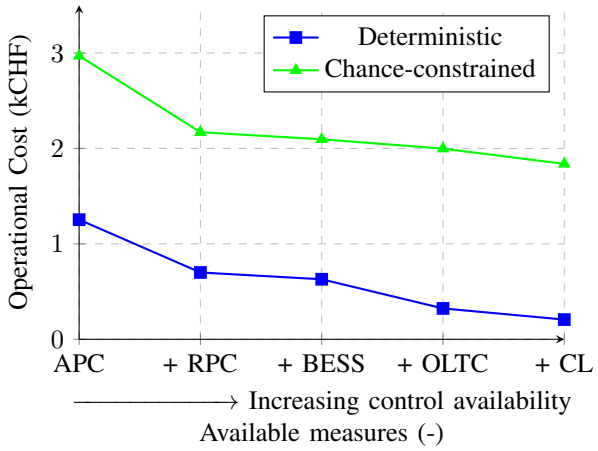

Fig. 10. Operational costs for different sets of active measures. APC = Active Power Curtailment, RPC = Reactive Power Control, BESS = Battery Energy Storage System, OLTC = On Load Tap Changing transformer, CL = Controllable Load

TABLE II
MAXIMUM PROBABILITY OF VOLTAGE AND THERMAL LOADING VIOLATION.

Available Measures	$\max(\mathbb{P}\{\lvert V_{\text{bus}}\rvert \leq V_{\max}\})$ (%) Uncertainty		$\max(\mathbb{P}\{\lvert I_{\text{br}}\rvert \leq I_{\text{i,max}}\})$ (%) Uncertainty	
	Without	With	Without	With
Active Power Curtailment	51	5	20	5
+ Reactive Power Control	35.6	4	51.7	5
+ BESS	35.6	4	51.7	5
+ OLTC transformer	48.9	4.8	52.8	5
+ Controllable Load	46.2	5	60.2	5

case where active power curtailment, reactive power control and BESS are the available active measures, and enforce the chance constraints with violation probability $\epsilon = 5\%$. We evaluate the behavior of the grid using 1000 samples from the forecast error distribution of Fig. 7c. The same samples are used for both optimization and evaluation to demonstrate that the method achieves the prescribed violation probability. Out-of-sample testing has been performed in earlier work [22].

Table II shows the maximum probability of overvoltage and thermal violation among all nodes and cables. Based on the examined 9-hours ahead forecast error distribution, the distribution network which does not consider uncertainties will face overvoltage and overload issues with a high probability (higher than 35% in most cases). The chance constraints limit this probability to 5% as prescribed by our choice of ϵ.

Figures 11 and 12 show the histograms of the voltage and current magnitudes at node 16 and cable $2-3$, respectively. Note that the consideration of the PV uncertainty through the chance constraints shifts the distribution to lower values, reducing both the probability of overvoltage and thermal overload to below the prescribed value.

4) Computational time and convergence characteristics of the proposed method: In this part, we elaborate on the convergence features and computational tractability of the iterative BFS-OPF. The proposed methodology is implemented in MATLAB using YALMIP [28] as the modeling layer, and

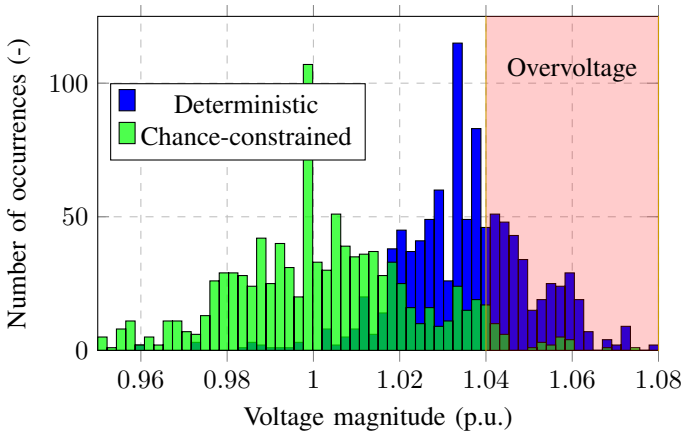

Fig. 11. Histograms of the voltage magnitudes at 14:00 at Node 16, evaluated based on Monte Carlo samples for both the deterministic (blue) and chance-constrained (green) solutions.

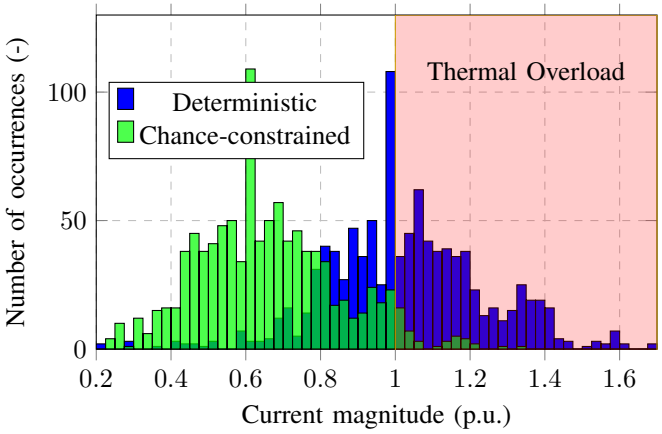

Fig. 12. Histogram of the current magnitudes at 14:00 at Cable $2-3$, evaluated based on Monte Carlo samples for both the deterministic (blue) and chance-constrained (green) solutions.

solved with Gurobi [29], using an Intel Core i7-2600 CPU and 16 GB of RAM.

Figure 13 shows the computational time needed for different available active measures. We observe a fairly constant burden for the deterministic case, where for all cases, almost the same number of iterations is needed until convergence, leading to similar computation times (see flowchart of the BFS-OPF). In the chance-constrained case, the more the available measures, the longer the time needed for the multi-period BFS-OPF. This can be explained by the consideration of more variables, in particular integer variables for the OLTC transformer and the controllable load. More iterations are needed in the chance-constrained case due to the second iteration loop which updates the constraints tightenings.

Finally, Figs. 14 and 15 provide insights in terms of the convergence characteristics of the proposed methodology. Without considering uncertainty, only the multi-period BFS-OPF loop is applied and, as can be observed in Fig. 14 for $m = 1$ (only this part is relevant for the deterministic case), convergence is reached after 4 iterations. The maximum voltage magnitude deviation of the first iteration for $k = 1$ is

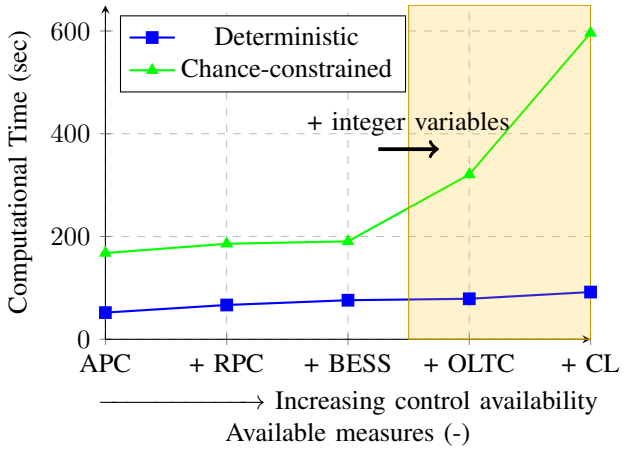

Fig. 13. Computational time needed for different sets of active measures. APC = Active Power Curtailment, RPC = Reactive Power Control, BESS = Battery Energy Storage System, OLTC = On Load Tap Changing transformer, CL = Controllable Load

large due to the initial flat voltage profile. From the second iteration on, i.e. from $k = 2$, the maximum voltage magnitude deviation is rather small, and the BFS-OPF converges after 4 iterations, when the maximum deviation is below the threshold of $\tilde{\eta} = 10^{-4}$.

In the chance-constrained case, after the voltage magnitudes have converged, the voltage and current uncertainty tightenings are checked for convergence. Once these tightenings are updated, the BFS-OPF iteration loop is run again, which increases the computational time compared to the deterministic case. Figure 14 shows the maximum voltage magnitude deviation for all iterations of the BFS-OPF loop. Note that the iterations until the first BFS-OPF convergence, i.e. $k \in \{1, 2, 3, 4\}$ and $m = 1$ are identical with the deterministic case, because of the same voltage initialization. Subsequently, the voltage and current uncertainty tightenings are updated, since they deviate more than the predefined thresholds of $\eta_V^{\Omega} = \eta_I^{\Omega} = 10^{-3}$, as can be observed in Fig. 15. The second run of the BFS-OPF loop for $m = 2$ converges faster, namely after 3 iterations, due to a better initial voltage profile. In total 4 iterations of the uncertainty tightening loop are needed in order to reach convergence of both loops.

VIII. Conclusion

In this paper, we propose a chance constrained multi-period optimal power flow algorithm, which can be used in the operational planning procedure of active distribution networks under uncertainty. The tractability is achieved by using an iterative power flow approach and the consideration of uncertainty is based on uncertainty margins calculated by Monte Carlo simulations.

In the case study considered, we provide results concerning the utilization of various sets of active measures, and the importance of accounting for uncertainty in terms of constraint violation and cost increase. The more the available measures, the lower the operational costs, with reactive power control

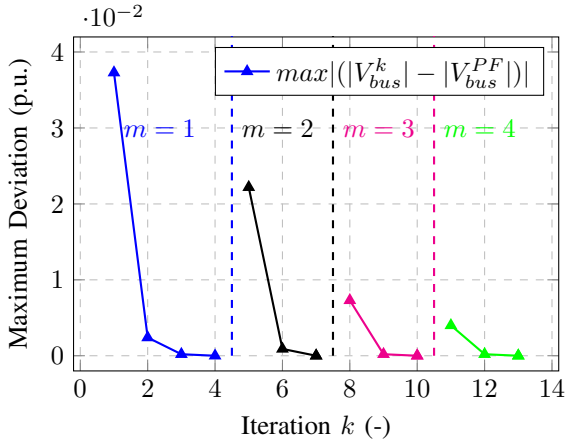

Fig. 14. Voltage magnitude convergence of the BFS-OPF loop. The deterministic case corresponds to the first iteration $m = 1$, plotted in blue. The chance-constrained optimization requires several outer iterations $m = 1, 2, 3, 4$ to achieve convergence of the tightenings.

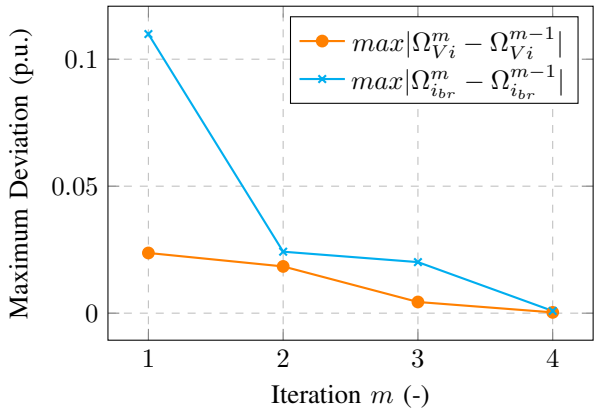

Fig. 15. Convergence of the voltage and current tightenings in the chance-constrained optimization. Maximum change in the voltage tightenings (plotted in orange) and current tightenings (in blue) between subsequent outer iterations m.

being the most efficient measure. The consideration of uncertainty more than doubles the operational cost, but limits the constraint violation probability to less than a predetermined value. Finally, we elaborate on the algorithmic performance of the proposed iterative method. Future work will focus on evaluating the convergence and optimality of the obtained solutions compared to full AC OPF and common convex relaxation techniques.

References

[1] P. Kotsampopoulos, N. Hatziargyriou, B. Bletterie, and G. Lauss, "Review, analysis and recommendations on recent guidelines for the provision of ancillary services by Distributed Generation," in *IEEE International Workshop on Intelligent Energy Systems, IWIES*, 2013, pp. 185–190.

[2] R. Tonkoski, L. A. C. Lopes, and T. H. M. El-Fouly, "Coordinated active power curtailment of grid connected PV inverters for overvoltage prevention," *IEEE Transactions on Sustainable Energy*, vol. 2, no. 2, pp. 139–147, 2011.

[3] S. Karagiannopoulos, P. Aristidou, and G. Hug, "Co-optimisation of Planning and Operation for Active Distribution Grids," in *Proceedings of the 12th IEEE Power and Energy Society PowerTech Conference, Manchester*, Jun 2017.

[4] E. Vrettos and G. Andersson, "Scheduling and Provision of Secondary Frequency Reserves by Aggregations of Commercial Buildings," *IEEE Transactions on Sustainable Energy*, vol. 7, no. 2, pp. 850–864, 2016.

[5] S. Weckx, C. Gonzalez, and J. Driesen, "Combined central and local active and reactive power control of PV inverters," *IEEE Transactions on Sustainable Energy*, vol. 5, no. 3, pp. 776–784, 2014.

[6] P. Fortenbacher, M. Zellner, and G. Andersson, "Optimal sizing and placement of distributed storage in low voltage networks," in *Proceedings of the 19th Power Systems Computation Conference (PSCC), Genova*, Jun 2016.

[7] S. Karagiannopoulos, P. Aristidou, A. Ulbig, S. Koch, and G. Hug, "Optimal planning of distribution grids considering active power curtailment and reactive power control," *IEEE Power and Energy Society General Meeting*, 2016.

[8] S. Karagiannopoulos, P. Aristidou, and G. Hug, "Hybrid approach for planning and operating active distribution grids," *IET Generation, Transmission & Distribution*, pp. 685–695, Feb 2017.

[9] E. Demirok, P. C. González, K. H. B. Frederiksen, D. Sera, P. Rodriguez, and R. Teodorescu, "Local reactive power control methods for overvoltage prevention of distributed solar inverters in low-voltage grids," *IEEE Journal of Photovoltaics*, vol. 1, no. 2, pp. 174–182, 2011.

[10] E. Dall' Anese, S. V. Dhople, and G. B. Giannakis, "Optimal Dispatch of Photovoltaic Inverters in Residential Distribution Systems," *IEEE Transactions on Sustainable Energy*, vol. 5, no. 2, pp. 487–497, 2014.

[11] E. Dall' Anese, S. V. Dhople, B. B. Johnson, and G. B. Giannakis, "Optimal Dispatch of Residential Photovoltaic Inverters Under Forecasting Uncertainties," *IEEE Journal of Photovoltaics*, vol. 5, no. 1, pp. 350–359, Jan 2015.

[12] P. Fortenbacher, A. Ulbig, and G. Andersson. Optimal Placement and Sizing of Distributed Battery Storage in Low Voltage Grids for Receding Horizon Control Strategies. [Online]. Available: https://arxiv.org/abs/1609.07128

[13] E. Dall Anese, K. Baker, and T. Summers, "Chance-Constrained AC Optimal Power Flow for Distribution Systems with Renewables," *IEEE Transactions on Power Systems*, 2017.

[14] J. Lavaei and S. H. Low, "Zero duality gap in optimal power flow problem," *IEEE Transactions on Power Systems*, vol. 27, no. 1, pp. 92–107, 2012.

[15] J. H. Teng, "A direct approach for distribution system load flow solutions," *IEEE Transactions on Power Delivery*, vol. 18, no. 3, pp. 882–887, 2003.

[16] L. Roald, F. Oldewurtel, T. Krause, and G. Andersson, "Analytical reformulation of security constrained optimal power flow with probabilistic constraints," in *Proceedings of the 10th IEEE Power and Energy Society PowerTech Conference, Grenoble*, Jun 2013.

[17] Haoyuan Qu, L. Roald, and G. Andersson, "Uncertainty margins for probabilistic AC security assessment," in *Proceedings of the 11th IEEE Power and Energy Society PowerTech Conference, Eindhoven*, Jun 2015.

[18] J. Schmidli, L. Roald, S. Chatzivasileiadis, and G. Andersson, "Stochastic AC optimal power flow with approximate chance-constraints," in *IEEE Power and Energy Society General Meeting (PESGM)*, Jul 2016.

[19] K. Baker, E. Dall'Anese, and T. Summers, "Distribution-agnostic stochastic optimal power flow for distribution grids," in *Proceedings of North American Power Symposium (NAPS)*, Sep 2016.

[20] M. Vrakopoulou, M. Katsampani, K. Margellos, J. Lygeros, and G. Andersson, "Probabilistic security-constrained AC optimal power flow," in *IEEE PowerTech Conference*, Grenoble, France, June 2013.

[21] K. Baker and B. Toomey. (2016) Efficient Relaxations for Joint Chance Constrained AC Optimal Power Flow. [Online]. Available: http://arxiv.org/abs/1608.08247

[22] L. Roald and G. Andersson, "Chance-Constrained AC Optimal Power Flow: Reformulations and Efficient Algorithms," Jun. 2017. [Online]. Available: https://arxiv.org/abs/1706.03241

[23] VDE-AR-N 4105, "Power generation systems connected to the LV distribution network." FNN, Tech. Rep., 2011.

[24] V. Poulios, E. Vrettos, F. Kienzle, E. Kaffe, H. Luternauer, and G. Andersson, "Optimal placement and sizing of battery storage to increase the PV hosting capacity of low voltage grids," in *International ETG Congress 2015, Die Energiewende - Blueprints for the new energy age*, 2015.

[25] L. Roald, F. Oldewurtel, B. Van Parys, and G. Andersson, "Security Constrained Optimal Power Flow with Distributionally Robust Chance Constraints," pp. 1–8, aug 2015. [Online]. Available: http://arxiv.org/abs/1508.06061

[26] K. Strunz, E. Abbasi, C. Abbey, C. Andrieu, F. Gao, T. Gaunt, A. Gole, N. Hatziargyriou, and R. Iravani, "Benchmark Systems for Network Integration of Renewable and Distributed Energy Resources," *CIGRE, Task Force C6.04*, no. 273, pp. 4–6, 4 2014.

[27] "MeteoSwiss - Federal Office of Meteorology and Climatology." [Online]. Available: http://www.meteoswiss.admin.ch/

[28] J. Löfberg, "Yalmip : A toolbox for modeling and optimization in matlab," in *In Proceedings of the CACSD Conference*, Taipei, Taiwan, 2004.

[29] I. Gurobi Optimization, "Gurobi optimizer reference manual," 2016. [Online]. Available: http://www.gurobi.com